nature portfolio

Peer Review File

Dual-domain solvent-locked electrolyte enabled durable 4.5 V-class sodium batteries

Corresponding Author: Professor Weihua Chen

This file contains all reviewer reports in order by version, followed by all author rebuttals in order by version.

Version 0:

Reviewer comments:

Reviewer #1

(Remarks to the Author)
The manuscript reports a novel electrolyte design, dual-domain solvent-locked electrolyte, achieving stable cycling of sodium-ion batteries at high voltage. Through a combination of systematic experimental investigation and theoretical analysis, the study elucidates the profound impact of the electrolyte design in significantly boosting electrochemical stability at bulk-phase electrolyte and cathode interface, and demonstrates a linear relationship between theoretical bandgap value and experimental oxidation decomposition of CEI components. These findings are highly instructive for the design of highly stable electrolytes and interphases. However, to meet the rigorous standards of high-impact academic publications, certain details and expressions require further polishing. Therefore, this manuscript is suggested to be accepted after a minor revision.
The suggested revisions are as follows:
1. The solvent-reinforced solvation structure proposed in this work appears conceptually opposite to the previously reported weak-solvation structures. However, both approaches improve electrolyte stability. It would be beneficial to provide a comprehensive and clear explanation delineating the key differences between these two strategies, and elaborating on the reasons for the seemingly paradoxical phenomenon.
2. NaDFOB also serves as an effective sodium electrolyte salt. When used as the sole electrolyte salt in the existing solvent formulation, is it capable of achieving high oxidation stability? Compared to the NaPF6+NaDFOB electrolyte, what are the differences in the solvation configuration, interphase structure, and battery performance when NaDFOB is used alone?
3. On line 80, the authors claim good separator wettability for the baseline electrolyte. However, supporting evidence for this claim appears to be lacking in the manuscript. Furthermore, upon increasing the concentration of the additional salt, is this wettability maintained?
4. The authors should discuss the mechanisms underlying overcharge and capacity fading observed during charge/discharge cycling in the baseline electrolyte, and the role of the dual-domain solvent-locked electrolyte in mitigating it.
5. The manuscript reports high ionic conductivity for the baseline electrolyte, yet Figure 1a shows a drop in conductivity with the addition of low-concentration NaDFOB. Can this discrepancy be clarified?
6. In Experimental section, the key high-voltage cathode material (Na2.26Fe1.87(SO4)3) requires clarification regarding its source and structure characteristics.

Reviewer #2

(Remarks to the Author)
Sodium iron sulfate (NFS) cathodes are considered among the most promising candidates for sodium-ion batteries owing to their exceptionally low raw-material cost. However, their practical application is severely hindered by poor cycling stability at high cut-off voltages (e.g., 4.5 V), primarily caused by pronounced parasitic reactions between the cathode and electrolyte, which limit full utilization of the theoretical capacity. In this work, the authors report a dual-domain solvent-locked electrolyte that effectively enhances oxidative stability and interfacial robustness, enabling stable operation of 4.5-V-class NFS sodium-ion batteries. The topic is timely and scientifically significant, and the demonstrated long-term cycling performance exceeding 16,000 cycles is particularly impressive. Overall, the manuscript is clearly written and well discussed. I would recommend acceptance after the following comments are adequately addressed.

1. The authors emphasize the role of DFOB anions in enabling ester molecular locking to enhance oxidation stability of the electrolyte. Is there a discernible trend in oxidation stability with varying DFOB concentrations?
2. Could this electrolyte design strategy be extended to other battery systems? Providing examples demonstrating its applicability beyond the current system would strengthen the manuscript's impact.
3. The authors correlate the electron tunneling probability of the CEI with the bandgap of its components. However, the underlying physical mechanism linking bandgap to tunneling probability, specifically concerning electronic transitions, remains incompletely elucidated.
4. A significant overcharge phenomenon is observed in the mass spectrometry experiment using the baseline electrolyte (Fig. 2g). However, the electrochemical testing in coin cell (Fig. 6g) shows a less pronounced overcharge effect, allowing for cycling beyond 50 cycles. Please clarify this apparent discrepancy in detail.
5. The data points in Figure 6b representing comparative performance lack clear sourcing and context. Adding a supplementary table listing the corresponding references and key parameters (e.g., cycle lifetime, charging rate, specific electrolyte used) for each data would significantly improve clarity.
6. While the supporting information is detailed, error bars or statistical analysis are absent for critical metrics including ionic conductivity, transference number, and oxidation window. Providing reproducibility data and uncertainty analysis is essential to strengthen scientific reliability. Furthermore, it remains unclear whether the enhanced oxidation stability extends to alternative substrates used as the working electrode instead of steel sheet.
7. Experimental details:
a. A more detailed description of how the cathode–electrolyte composite model was constructed and the kinetic optimization procedures applied.
b. The scan rates used in LSV, in situ characterizations, and other electrochemical tests should be specified.
c. Detailed procedures for XRD testing and refinement should be described.
d. The caption for Supplementary Figure 3 is currently missing and needs to be provided.

Reviewer #3

(Remarks to the Author)
The manuscript reports a NaDFOB/NaPF6-based carbonate electrolyte that enables high-voltage, long-life sodium metal batteries. This electrolyte shows excellent electrochemical properties and can stabilize both the SEI on Na metal and the CEI on a 4.5 V cathode. The working mechanism is systematically investigated through experimental analyses and theoretical calculations. These findings provide an important reference for designing electrolytes suitable for high-voltage sodium batteries. The revision comments are as follows:

1. The meanings of "dual-domain" and "solvent-locked" are not clearly explained. Please clarify where the "dual domains" are in the NaDFOB–NaPF6 electrolyte, and how the solvent is "locked."

2. For Na-metal coin cells, why was a glass-fiber membrane used instead of conventional PP separators? In contrast, the pouch cells use a PP separator.

3. How does adding NaDFOB affect the electrolyte viscosity? Please show the viscosity data of the electrolytes listed in Figure 1a.

4. In Figure 3a, NaDFOB decomposes at a low voltage of 2.9 V. Since NaDFOB is a component of the DDSLE, it is not appropriate to claim that the decomposition voltage of this electrolyte is 5.1 V.

Version 1:

Reviewer comments:

Reviewer #1

(Remarks to the Author)
The authors have addressed the comments and revised the manuscript accordingly. I would like to recommend the publication of the work in the current form.

Reviewer #2

(Remarks to the Author)
The authors have addressed all comments. I recommend to publishing it

Reviewer #3

(Remarks to the Author)
All questions have been addressed. The revised manuscript is recommended for publication.

Point-by-point response to the reviewers' Comments

Response to Reviewer 1:

The manuscript reports a novel electrolyte design, dual-domain solvent-locked electrolyte, achieving stable cycling of sodium-ion batteries at high voltage. Through a combination of systematic experimental investigation and theoretical analysis, the study elucidates the profound impact of the electrolyte design in significantly boosting electrochemical stability at bulk-phase electrolyte and cathode interface, and demonstrates a linear relationship between theoretical bandgap value and experimental oxidation decomposition of CEI components. These findings are highly instructive for the design of highly stable electrolytes and interphases. However, to meet the rigorous standards of high-impact academic publications, certain details and expressions require further polishing. Therefore, this manuscript is suggested to be accepted after a minor revision.

Answer: We thank the reviewer for their thorough review and positive evaluation of our work. We have carefully refined and polished the details and expressions in the revised manuscript to ensure it meets the journal's publication standards.

The suggested revisions are as follows:

Question 1. The solvent-reinforced solvation structure proposed in this work appears conceptually opposite to the previously reported weak-solvation structures. However, both approaches improve electrolyte stability. It would be beneficial to provide a comprehensive and clear explanation delineating the key differences between these two strategies, and elaborating on the reasons for the seemingly paradoxical phenomenon.

Answer: Thank you for your insightful and constructive comment. The fact that both strategies significantly enhance electrolyte stability stems from their targeted optimization of distinct dominant failure mechanisms within the electrochemical system. Their core difference lies in the deliberate design of the solvation structure, both ultimately promote stability by enabling effective interfacial protection.

(1) Explanation of the seemingly contradictory phenomenon

(a) Solvent-reinforced strategy

Structural feature: a compact, thermodynamically stable solvation sheath dominated by solvents.

Typical implementation: using high-donor-number solvents or specific coordinating molecules.

Key design principle: strengthening the interaction between solvent and cation.

Stability mechanism: this structure directly improves the intrinsic oxidation resistance of the electrolyte by lowering HOMO energy level of the coordinated solvent-cation unit. Additionally, the "locked" solvent molecules within the sheath reduce side reactions caused by their free movement.

(b) Weakly solvating strategy

Structural feature: a loose solvation sheath, where anions enter the inner coordination sphere.

Typical implementation: employing low-donor-number solvents or high-concentration electrolytes.

Key design principle: weakening solvent-cation binding to promote anion participation in solvation.

Stability mechanism: this approach shifts the HOMO location of solvation sheath from the solvent towards the salt (*Nat. Energy*, **2019**, 4, 269–280). This induces the preferential decomposition of anions at interfaces, forming a dense, ion-conductive interphases while kinetically suppressing solvent decomposition.

While the core design principles (strengthening *vs.* weakening solvent-cation binding) are indeed opposing, the fundamental distinction lies in actively controlling the coordination competition within the cation's primary solvation shell to dictate interfacial reaction pathways.

(2) Explanation for the enhanced electrolyte stability

The key to understanding this seemingly contradictory phenomenon lies in recognizing that both strategies achieve the same ultimate goal—constructing a stable electrode/electrolyte interface via fundamentally different pathways. They address the problem from two complementary dimensions: thermodynamics and kinetics.

(a) Solvent-reinforced strategy

This strategy primarily focuses on thermodynamic stability. It creates a more inert bulk electrolyte by reducing the reactivity of its components. Its robust solvation sheath undergoes a controlled, orderly decomposition at interfaces, tending to yield thin and uniform interphase layers.

(b) Weakly solvating strategy

This strategy primarily excels at kinetic optimization. By lowering the desolvation energy barrier, it enhances ion transport kinetics. Crucially, it regulates the decomposition sequence, allowing anions sacrificed to form high-quality interphases during interfacial reaction, thereby kinetically protecting the solvent molecules.

In summary, the "solvent-reinforced" and "weakly solvating" strategies are not opposing but represent two distinct, effective pathways in electrolyte engineering. The former enhances intrinsic stability by strengthening internal bonds, while the latter guides the formation of ideal interphase by optimizing reaction sequence and kinetics. Their collective success reaffirms the core principle that the electrode/electrolyte interface ultimately dictates battery performance.

On page 4 of revised manuscript, we have added the discussion with "In terms of fundamental design and mechanism, the "solvent-reinforced" and "weakly solvating" strategies are not opposing but represent two distinct, effective pathways in electrolyte engineering (Supplementary note 2). The former enhances intrinsic stability by strengthening internal bonds, while the latter guides the formation of ideal interphase by optimizing reaction sequence and kinetics.".

On page 33 of revised Supplementary information, we have added the discussion as Supplementary note 2.

Question 2. NaDFOB also serves as an effective sodium electrolyte salt. When used as the sole electrolyte salt in the existing solvent formulation, is it capable of achieving high oxidation stability? Compared to the $NaPF_6$+NaDFOB electrolyte, what are the differences in the solvation configuration, interphase structure, and battery performance when NaDFOB is used alone?

Answer: Thanks for your professional advice. As suggested, we conducted an in-depth study of the single-salt electrolyte (0.4M NaDFOB in EC/EMC, denoted as DE) and systematically compared its properties and performance characteristics with those of the DDSLE electrolyte (1M $NaPF_6$ + 0.4M NaDFOB in EC/EMC) and BE electrolyte (1M $NaPF_6$ in EC/EMC). The key findings are as follows:

(1) Oxidation stability

The DE electrolyte exhibits high intrinsic stability, with an anodic stability limit of 4.8 V, as demonstrated by linear sweep voltammetry (LSV) curves in **Figure R1a**. However, the onset of oxidation occurs at a lower potential (around 3.8 V), which correlates with the progressive decomposition of the $DFOB^-$ anion. This indicates that NaDFOB alone provides sufficient intrinsic protection against oxidation but may not achieve the same level of stability as the mixed DDSLE system.

(2) Solvation configuration

Both the DE and DDSLE electrolytes exhibit similar anion coordination behaviors. Molecular

dynamics simulations reveal that the $DFOB^-$ anions predominantly reside in the outer solvated Na^+ shell and do not participate in the inner-shell coordination (**Figures R1b–d**). This consistent solvation behavior suggests that NaDFOB's solvation properties are comparable to those in the DDSLE system.

(3) Interphase structure

This is the core factor responsible for the performance divergence between the two electrolytes. Although the decomposition products of $DFOB^-$ (e.g., NaF, borates) are electrochemically stable, their interphase-forming processes and final morphologies differ fundamentally.

In the DE electrolyte, the cathode electrolyte interphase (CEI) and solid electrolyte interphase (SEI) are highly inhomogeneous and physically unstable (**Figures R2a–b**). These interphases fail to provide effective passivation of the cathode or the Na anode, leading to electrolyte decomposition and gas release (**Figure R2c**). Additionally, the interphases exhibit poor mechanical stability, prone to fracture and dissolution during cycling, as evidenced by EQCM measurements (**Figure R2d**).

In the DDSLE system, a sequential and synergistic decomposition occurs involving $DFOB^-$, PF_6^-, and solvents, resulting in the formation of a dense inorganic-rich inner layer and a flexible outer layer. This optimized interphase provides a balanced ionic conductivity and mechanical toughness, ultimately enabling the DDSLE system to achieve an ultra-long cycling life of over 16,500 cycles at 10C.

(4) Battery performance: contrast in reversibility and durability

The DE electrolyte supports a reversible Na (de)intercalation in NFS cathode, with an initial Coulombic efficiency of 90.5%, confirming its fundamental electrochemical compatibility (**Figure R3a**). However, its cell capacity decays rapidly after approximately 1500 cycles due to the inhomogeneous and unstable interphase to provide lasting protection (**Figure R3b**).

In summary, while NaDFOB as the sole electrolyte salt offers a wide electrochemical window based on its high intrinsic oxidation stability, its interphase structure inherently lacks the homogeneity and mechanical stability required for long-term cycling performance. In contrast, the mixed-salt DDSLE system, on the other hand, leverages the unique properties of both $DFOB^-$ and PF_6^- to create an optimized interphase architecture. This strategy ensures superior intrinsic stability, interfacial protection, and overall battery performance.

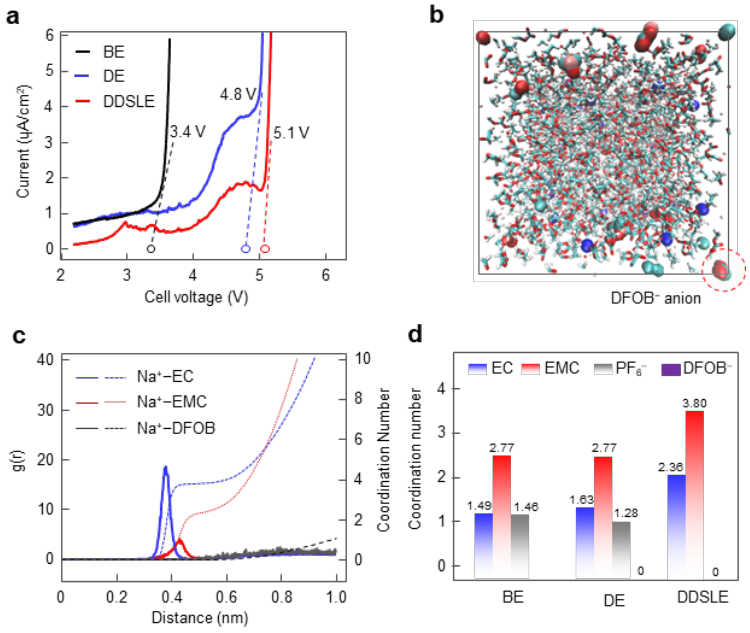

Figure R1. Oxidation stability and solvation structure of DE electrolyte. (a) LSV curves of three

electrolytes in Na||steel sheet cells. (b) Snapshots from MD simulations. (c) Radial distribution functions and coordination numbers. (d) Average coordination numbers obtained from MD simulations.

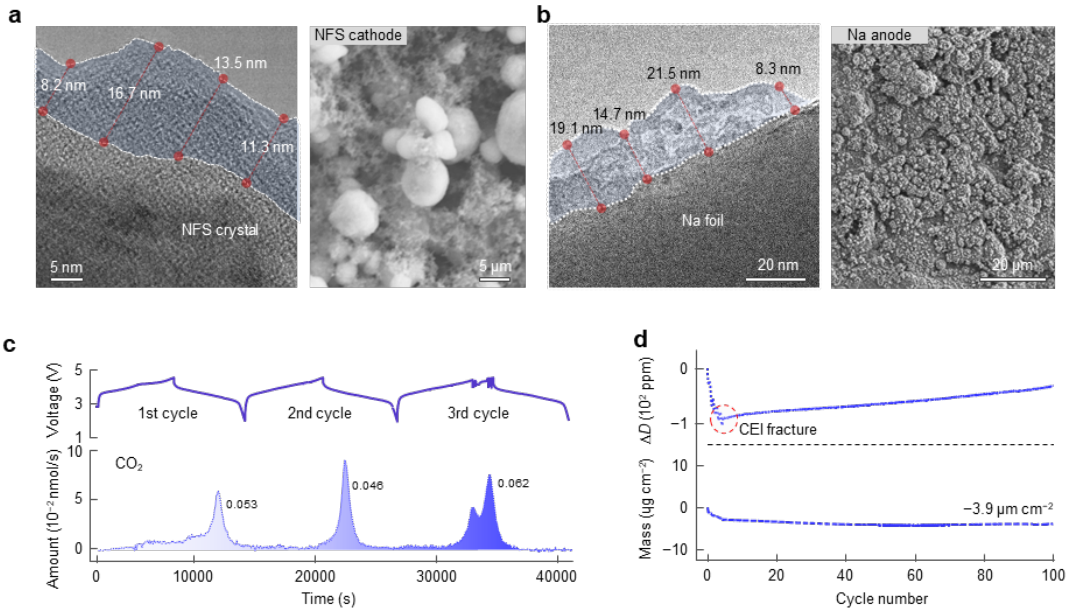

Figure R2. Interphase structure and mass evolution in DE electrolyte. TEM and SEM images of (a) NFS cathode and (b) Na anode after 3 cycles. (c) *In situ* DEMS data for Na||NFS cell. (d) Time-dependent changes in mass (Δm) and energy dissipation (ΔD) for a Na||NFS cell over multiple cycles during CV measurement recorded via *in situ* EQCM.

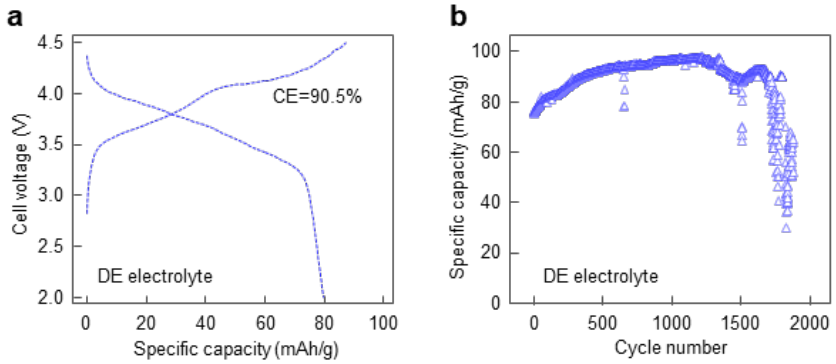

Figure R3. Cycling performance of Na||NFS cell in DE electrolyte. (a) Galvanostatic charge–discharge profiles at 1st cycle. (b) cycling performance of Na||NFS coin cells using DE electrolyte at 1C.

On page 8 of revised manuscript, we have added the discussion with "While using NaDFOB as the sole electrolyte salt features a high anodic stability limit, this advantage is negated by the formation of an uneven and mechanically unstable interphases, which prevents long-term high-voltage operation and limits the cycle life to only about 1500 cycles (Supplementary Fig. 21 and note 5)."

On page 22 of revised Supplementary information, we have added the Figures R1−3 in Supplementary Fig. 21.

On page 37 of revised Supplementary information, we have added the discussion as Supplementary note 5.

Question 3. On line 80, the authors claim good separator wettability for the baseline electrolyte. However, supporting evidence for this claim appears to be lacking in the manuscript. Furthermore, upon increasing the concentration of the additional salt, is this wettability maintained?

Answer: Thanks for your professional advice. As suggested, we conducted the contact angle tests of electrolytes on typical PP and glass fiber (GF) separators, whose results are presented in **Figure R4**.

After contacting the PP separator and reaching stabilization, the baseline electrolyte exhibited a contact angle of 61.6 °. Even with an increased concentration of NaDFOB in the electrolytes, the contact angle on PP separator remained consistently within a narrow range of 56.1 ° to 61.2 °. This suggests that the higher salt concentration did not impede the wettability between the electrolyte and the separator. In contrast, for the GF separator, electrolytes of all concentrations fully penetrated the fiber gaps within 1 second of contact, demonstrating excellent wettability and rapid absorption capability.

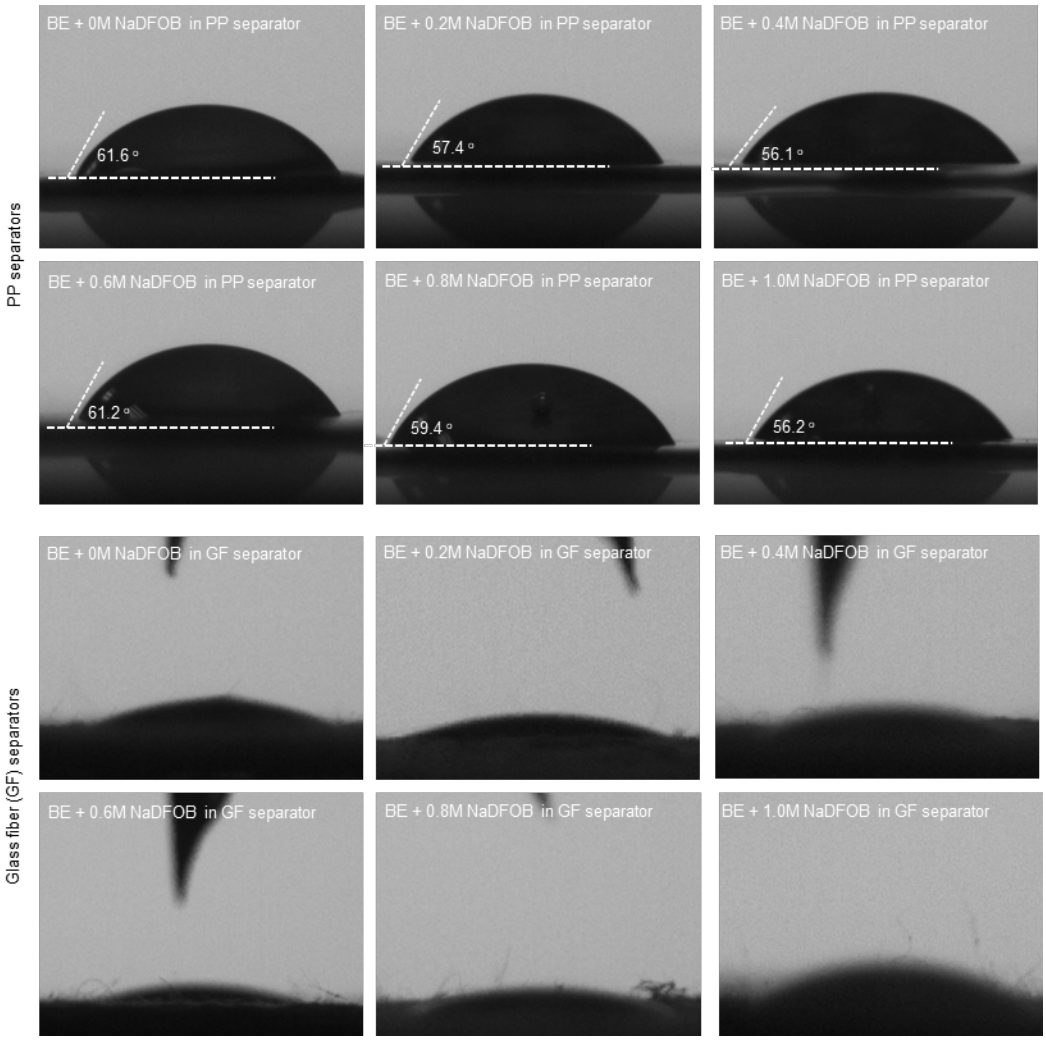

Figure R4. Contact angle test images of different electrolytes on PP and glass fiber separators.

On page 3 of revised manuscript, we have revised the discussion with "While BE electrolyte offers favorable ionic conductivity, low viscosity, and separator wettability, it exhibits poor high-voltage stability (~3.4 V *vs.* Na^+/Na).[11]".

On page 3 of revised Supplementary information, we have added the Figure R4 in Supplementary Fig. 2.

Question 4. The authors should discuss the mechanisms underlying overcharge and capacity fading observed during charge/discharge cycling in the baseline electrolyte, and the role of the dual-domain solvent-locked electrolyte in mitigating it.

Answer: Thanks for your valuable suggestion. As advised, we have conducted a comprehensive analysis of the baseline electrolyte (BE) and the dual-domain solvent-locked electrolyte (DDSLE), focusing on the mechanisms underlying overcharge and capacity fading. Related analysis is summarized as follows:

(1) Mechanisms of overcharge and capacity fading in BE electrolyte

(a) Thermodynamic origin of instability

The BE electrolyte exhibits thermodynamic instability due to its solvation structure dominated by carbonate solvents (EC/EMC). These solvents feature loose coordination and a high HOMO level (−7.92 eV), leading to a low intrinsic oxidation potential (as evidenced in Figure 3a of the revised manuscript). Upon charging at high voltages (>3.4 V *vs.* Na^+/Na), solvent molecules and PF_6^- anions undergo irreversible oxidative decomposition on the cathode surface.

(b) Defective cathode electrolyte interphase

The decomposition products form an initial CEI primarily composed of organic carbonates and polyesters. This CEI is structurally porous and inhomogeneous, failing to effectively passivate the cathode. The low electronic insulation of its components (narrow bandgap) exacerbates electron tunneling at high voltages, resulting in significant leakage current and uneven interfacial potential distribution (as shown in Figure 3e and 4c−d of the revised manuscript). This setup provides only transient protection, initiating a vicious cycle of parasitic reactions.

(c) Vicious cycle of parasitic reactions

The defective CEI offers limited protection against electrolyte decomposition, leading to a continuous "decomposition–thickening–fracturing–re-decomposition" cycle. Over time, mechanical stress fractures and dissolves the CEI, causing sharp increases in interfacial impedance (as demonstrated in Figure 6a of the revised manuscript). The cumulative effects of these processes ultimately manifest as:

"Overcharge" phenomenon: an extended voltage plateau or voltage rise in the voltage-capacity profile, wherein energy is wasted on parasitic reactions instead of contributing to useful capacity.

Rapid capacity fading: loss of active sodium, potential corrosion of the cathode material, and dissolution of transition metals from interfacial side reactions, coupled with blocked ion transport channels, lead to rapid capacity decay.

(2) Stabilization mechanism of DDSLE electrolyte

(a) Enhancing bulk thermodynamic stability

The $DFOB^-$ anion, through its non-solvating effect and large steric hindrance, drives electron density redistribution and stabilizes a solvent-reinforced solvation structure within the bulk electrolyte. This effectively lowers the HOMO energy level of the coordinated species (−8.22 eV), thereby elevating the intrinsic oxidation stability of the electrolyte.

(b) Guiding the construction of a robust and homogeneous interphase

The $DFOB^-$ anion preferentially adsorbs and decomposes on the cathode surface at voltages above its decomposition potential (3.0−3.6 V *vs.* Na^+/Na). Its decomposition products, primarily inorganic compounds with wide bandgaps and high ionic conductivity (e.g., NaF and borates), form a dense, uniform, and mechanically robust CEI. This layer effectively blocks direct cathode/electrolyte contact and suppresses electron tunneling, providing long-term protection against interfacial degradation (as demonstrated in Figures 3e and 4h of the revised manuscript).

(c) Suppressing parasitic reactions for long-term kinetic stability

The optimized CEI fundamentally curtails continuous electrolyte decomposition and gas generation. Its stable structure and chemical properties prevent fracture and reconstruction during cycling, ensuring long-term stability of the interfacial impedance (as demonstrated in Figure 2h and 6a of the revised manuscript). This eliminates the core drivers behind overcharge and capacity fading.

In summary, the failure of the baseline electrolyte stems from its thermodynamic instability and consequently sustained interfacial degradation. In contrast, the DDSLE electrolyte, through elaborate solvation structure design, redirects the interfacial formation process towards an orderly, controlled passivation guided by a specific anion. This achieves synergistic reinforcement at both the thermodynamic (enhancing intrinsic stability) and kinetic (constructing a stable interphase) levels, effectively resolving the issues of overcharge and rapid capacity fade at high voltages.

On page 8 of revised manuscript, we have revised the discussion with "Post-mortem analysis confirmed the interfacial integrity preserved by the DDSLE electrolyte, with electrodes and particles retaining their structure and separators remaining clean. In contrast, BE cells showed severe electrode pulverization, thick particle coatings, and brown deposits on separators (Fig. 6c), reflecting the baseline electrolyte's thermodynamic instability and the resulting cycle of sustained interfacial degradation it triggers. The minimal byproduct formation in DDSLE-involved cells signifies a stabilized internal environment during cycling, which is attributed to the DDSLE's ability to ensure reversible Na^+ transport by stabilizing the interface, suppressing electrolyte decomposition, and preventing byproduct accumulation. This performance stems from the elaborate solvation structure design, which redirects interfacial formation toward an orderly, controlled passivation guided by a specific anion, achieving synergistic reinforcement at both the thermodynamic (enhancing intrinsic stability) and kinetic (constructing a stable interphase) levels. Consequently, DDSLE effectively resolves issues of overcharge and rapid capacity fade at high voltages, with stability extending to 60 °C operation, where Na||NFS cells retain 95.2 % capacity after 180 cycles (Fig. 6d). Deposits on BE-involved separators reveal significant Fe dissolution (Supplementary Fig. 22), indicating byproduct-catalyzed decomposition of polyanionic frameworks within separator pores. Crucially, the boride/fluoride-rich CEI in DDSLE electrolyte further inhibits Fe dissolution/migration and enhances interfacial stability.".

Question 5. The manuscript reports high ionic conductivity for the baseline electrolyte, yet Figure 1a shows a drop in conductivity with the addition of low-concentration NaDFOB. Can this discrepancy be clarified?

Answer: Thank you for your careful observation and thoughtful question. The difference you noted between the baseline electrolyte's high ionic conductivity and the drop in conductivity upon adding low-concentration NaDFOB can be reasonably explained by analyzing the physicochemical properties of the mixed-salt system. Key observations and explanations are summarized as follows:

(1) Baseline electrolyte (1M $NaPF_6$ in EC/EMC)

The baseline electrolyte exhibits excellent ionic conductivity, with a value of 2.6 mS cm^{-1}. This is attributed to the high mobility and smaller molecular structure of PF_6^- anions in carbonate-based electrolytes. PF_6^- is known for its excellent ion-transport properties, making it an ideal anion in carbonate electrolytes.

(2) Mixed-salt electrolyte systems with NaDFOB

When a low concentration of NaDFOB (e.g., 0.2 mol L^{-1}) is added to the baseline electrolyte, the overall ionic conductivity decreases to 1.8 mS cm^{-1}. This reduction in conductivity can be attributed to

the following factors:

(a) Lower intrinsic ionic conductivity of NaDFOB. The $DFOB^-$ anion has a more complex molecular structure compared to PF_6^-, resulting in lower ion mobility. This is further enhanced by the anion's non-solvating nature and large steric bulk. In carbonate-based electrolytes, the conductivity of NaDFOB solutions is typically below 2 mS cm^{-1}, whereas $NaPF_6$ systems often achieve 2–4 mS cm^{-1}. Thus, the addition of NaDFOB to the mixed-salt system introduces charge carriers with lower mobility.

(b) Ion-pair interactions and migration hindrance. The addition of NaDFOB introduces ion-pair interactions in the mixed-salt system. At low concentrations, the $DFOB^-$ anions tend to reside outside the primary solvation shell of Na^+ ions, where they can hinder the movement of solvated Na^+ complexes, further suppressing ion migration and overall conductivity.

(c) Increased electrolyte viscosity. The addition of NaDFOB salt raises the solution viscosity (**Figure R5**), which directly lower ionic mobility and conductivity.

In summary, the high conductivity of the baseline electrolyte is attributed to the excellent ion-transport properties of $NaPF_6$, while the drop in conductivity upon adding low concentrations of NaDFOB results from the combined effects of its intrinsically lower conductivity, hindered ion migration, and increased viscosity.

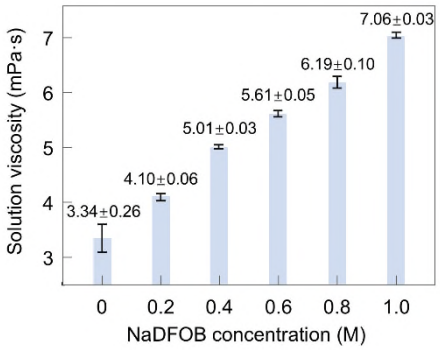

Figure R5. Viscosity of the baseline electrolyte (1M $NaPF_6$ EC/EMC) with different NaDFOB concentration.

On page 3 of revised manuscript, we have revised the discussion with "While BE electrolyte offers favorable ionic conductivity, low viscosity, and separator wettability, it exhibits poor high-voltage stability (~3.4 V *vs.* Na^+/Na).[11] Introducing low-concentration NaDFOB slightly reduced conductivity due to its lower intrinsic conductivity versus $NaPF_6$, hindered ion migration, and increased viscosity (Fig. 1a and Supplementary Figs. 1−2).".

On page 15 of revised manuscript, we have added the Figure R5 into the Figure 1a.

Question 6. In Experimental section, the key high-voltage cathode material ($Na_{2.26}Fe_{1.87}(SO_4)_3$) requires clarification regarding its source and structure characteristics.

Answer: We thank the reviewer for pointing out this missing information. We have supplemented the relevant material preparation process and structural characteristics.

The high-voltage cathode material, $Na_{2.26}Fe_{1.87}(SO_4)_3$/C, was synthesized via a modified co-precipitation route. The process begins with the dispersing of 0.3 g graphene oxide and 0.3 g Ketjen black in 60 mL deionized water under ultrasonication (100 W, 30 min; KQ-250DS, Kunshan Ultrasonic Instruments Co. Ltd.). This dispersion is then augmented with stoichiometric precursors, including 12 mmol Na_2SO_4, 18 mmol anhydrous $FeSO_4$, 0.3 g citric acid, and 0.12 g ascorbic acid, under continuous

stirring. The mixture undergoes low-temperature co-precipitation (<8 °C) via dropwise addition of 120 mL isopropanol, followed by sand milling (2000 rpm, 1 hour) to achieve uniform particle size. Subsequent spray-drying at 300 mL/hour yields a precursor, which is then calcined in Ar at 350 °C for 12 hours (2 °C/min ramp) to obtain the final composite material.

The resulting composite exhibits a hierarchical structure comprising hollow microspheres (0.5–10 μm diameter) with walls (50–200 nm thickness) constructed from NFS nanoparticles embedded in carbon matrix. This unique structure is validated by TEM elemental mapping, which shows a uniform distribution of Na/Fe/S/O across the material (**Figures R6a−b**). XRD analysis confirms the dominance of the $Na_{2.26}Fe_{1.87}(SO_4)_3$ phase as the primary crystalline component, characterized by a C2/c space group in monoclinic system (**Figure R6c**). The composite material's high 6.84 wt% carbon content forms a percolating conductive network, enhancing both electronic conductivity and ion diffusion kinetics (**Figure R6d**). This structural design is critical for enabling the reversible sodium storage capability of the material.

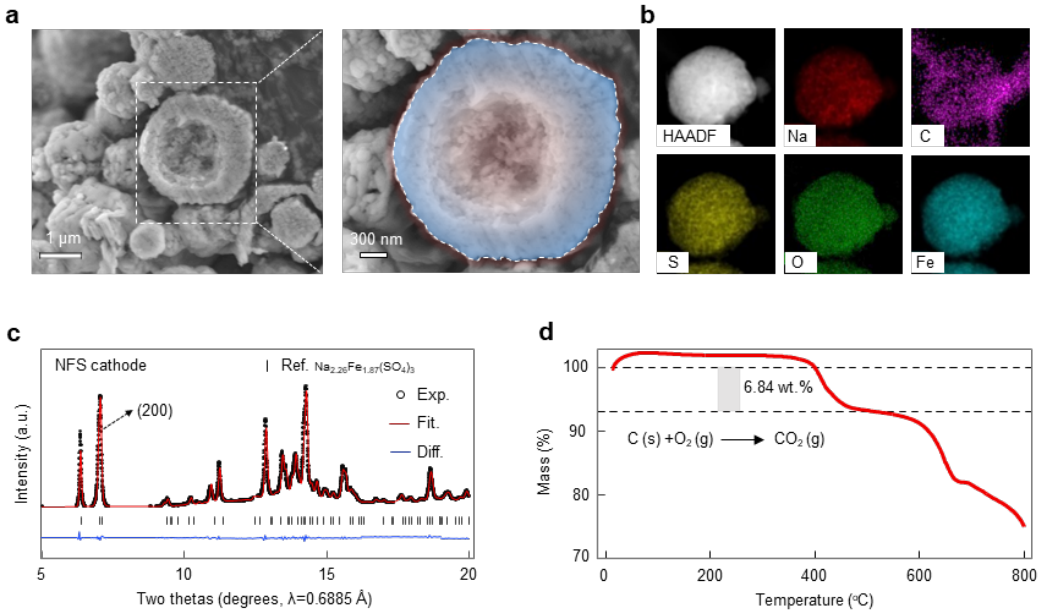

Figure R6. Structure characteristics of NFS cathode material. (a) SEM images. (b) Element mapping images. (c) X-ray diffraction Rietveld refinements. (d) Thermogravimetry curve.

On page 4 of revised manuscript, we have revised the discussion with "The alluaudite-type $Na_{2.26}Fe_{1.87}(SO_4)_3$ (NFS) cathode delivers a high average discharge voltage (3.8 V) and reversible specific capacity within 2.0–4.5 V.[17] Detailed structural characteristics are provided in Supplementary Fig. 8 and table 1. The (200) plane with well-ordered monoclinic atomic arrangement, identified as the dominant exposed facet via XRD refinement and high-resolution transmission electron microscopy (HRTEM) (spacing: 5.54 Å; C2/c space group, Fig. 2a), was selected as substrate model for simulating electrolyte contact due to its structural sensitivity and signal clarity.[18]"

On page 9−10 of revised manuscript, we have added the material preparation process with "The NFS was synthesized via a modified co-precipitation route initiated by dispersing 0.3 g graphene oxide and 0.3 g Ketjen black in 60 mL deionized water under ultrasonication (100 W, 30 min; KQ-250DS, Kunshan Ultrasonic Instruments Co. Ltd.). To this dispersion, stoichiometric precursors (12 mmol Na_2SO_4, 18 mmol $FeSO_4$), along with 0.3 g citric acid and 0.12 g ascorbic acid were added under

continuous stirring. The mixture underwent low-temperature co-precipitation (<8 ºC) via dropwise addition of 120 mL isopropanol, followed by sand milling (2000 rpm, 1 hour; nano sanding machine 30 L, Kunshan Zhuowei Machinery Technology Co. Ltd.) to homogenize particle size. Subsequent spray-drying at 300 mL/hour (TENLIN-6000Y, Jiangsu Tianling Instrument Co. Ltd.) yielded a precursor that was calcined in Ar at 350 ºC for 12 hours (2 ºC /min ramp) to crystallize the final NFS material.".

On page 9 of revised Supplementary information, we have added the Figure R6 in Supplementary Fig. 8.

All changes are marked in yellow in the revised manuscript for reference.

Response to Reviewer 2:

Sodium iron sulfate (NFS) cathodes are considered among the most promising candidates for sodium-ion batteries owing to their exceptionally low raw-material cost. However, their practical application is severely hindered by poor cycling stability at high cut-off voltages (e.g., 4.5 V), primarily caused by pronounced parasitic reactions between the cathode and electrolyte, which limit full utilization of the theoretical capacity. In this work, the authors report a dual-domain solvent-locked electrolyte that effectively enhances oxidative stability and interfacial robustness, enabling stable operation of 4.5-V-class NFS sodium-ion batteries. The topic is timely and scientifically significant, and the demonstrated long-term cycling performance exceeding 16,000 cycles is particularly impressive. Overall, the manuscript is clearly written and well discussed. I would recommend acceptance after the following comments are adequately addressed.

Answer: We thank the reviewer for their thorough review and positive evaluation of our work. We have carefully refined and polished the details and expressions in the revised manuscript to ensure it meets the journal's publication standards.

Question 1. The authors emphasize the role of DFOB anions in enabling ester molecular locking to enhance oxidation stability of the electrolyte. Is there a discernible trend in oxidation stability with varying DFOB concentrations?

Answer: Thanks for your valuable comments. We further evaluated the oxidation stability of electrolytes with varying NaDFOB concentrations, and the results demonstrate a clear trend.

(1) Enhanced oxidation stability with increasing NaDFOB concentration

LSV curves reveal a strong dependence of oxidation stability on NaDFOB concentration (**Figure R7**). The baseline electrolyte (BE, without NaDFOB) begins to decompose at approximately 3.4 V. Upon adding 0.2M NaDFOB, a new oxidation peak emerges between 3.0 and 3.6 V, corresponding to the preferential decomposition of $DFOB^-$ anions. By applying a threshold current density of 10 μA cm^{-2}, its anodic stability limit is determined to be 4.7 V. When the NaDFOB concentration is increased to 0.4M, the pre-decomposition peak at 3.0 V is suppressed to below 1.8 μA cm^{-2}, and the anodic stability limit is significantly raised to 5.1 V. Further increases in NaDFOB concentration are limited by salt solubility, leading to precipitate formation and no further improvement in oxidation limit.

(2) Underlying mechanism

This trend is attributed to the distinct roles of $DFOB^-$ anions within the bulk electrolyte and at the cathode interface.

In the baseline electrolyte (BE) without NaDFOB, oxidation decomposition is governed by a loosely coordinated carbonate-based solvation sheath and abundant free solvent molecules, leading to the oxidation at relatively low voltages.

At a low NaDFOB concentration (0.2M), the limited $DFOB^-$ anions are insufficient to concurrently establish a solvent-reinforced Na^+ solvation structure with bulk solution and anion-rich shield at the cathode interface. Consequently, most $DFOB^-$ anions preferentially accumulate and decompose at the cathode surface due to their strong binding affinity toward Na^+. However, the resulting insoluble products cannot form an integrated passivation interphase, resulting in partial decomposition of coordinated and free solvent molecules.

When the NaDFOB concentration reaches 0.4M, sufficient $DFOB^-$ anions enables the establishment of a dual-domain solvent-locked effect. This dual-domain solvent-locked effect significantly restricts the degrees of freedom and reactivity of the solvent molecules, thereby raising the anodic stability limit to 5.1 V and inhibiting subsequent decomposition of other electrolyte components.

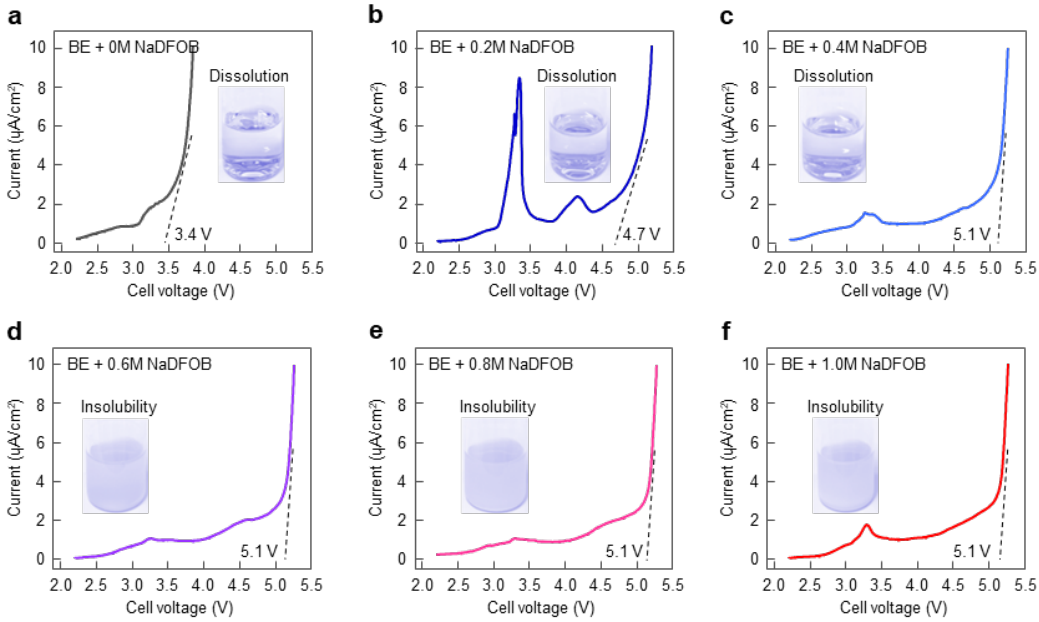

Figure R7. LSV curves of electrolytes with varying DFOB concentrations. (a) 0M. (b) 0.2M. (c) 0.4M. (d) 0.6M. (e) 0.8M. (f) 1.0M. Inset: digital photos of the electrolytes.

On page 3 of revised manuscript, we have revised the discussion with "While BE electrolyte offers favorable ionic conductivity, low viscosity, and separator wettability, it exhibits poor high-voltage stability (~3.4 V *vs.* Na^+/Na).[11] Introducing low-concentration NaDFOB slightly reduced conductivity due to its lower intrinsic conductivity versus $NaPF_6$, hindered ion migration, and increased viscosity (Fig. 1a and Supplementary Fig. 1). Importantly, at this concentration (0.2M), NaDFOB addition fails to satisfactorily enhance the electrolyte's anodic stability limit, primarily because it cannot sufficiently control the structure within the bulk electrolyte and at the cathode interface (Supplementary note 1). Higher NaDFOB concentrations modestly recovered conductivity and further increased viscosity, but beyond 0.6M, electrolyte cloudiness indicated salt precipitation.".

On page 2 of revised Supplementary information, we added the Figure R7 into Supplementary Fig. 1.

On page 32 of revised Supporting Information, we have added the discussion as Supplementary note 1.

Question 2. Could this electrolyte design strategy be extended to other battery systems? Providing examples demonstrating its applicability beyond the current system would strengthen the manuscript's impact.

Answer: We appreciate the reviewer's insightful suggestion. We have extended our dual-domain molecular-locked strategy to other battery systems (**Figure R8**), as detailed below:

(a) For carbonate-based electrolytes in lithium-ion batteries (BE1: 1.2M $LiPF_6$ EC/EMC/DMC), we utilize a concentration of 0.2M DFOB additive and achieved an anodic stability limit increase from 4.0 V to 5.0 V.

(b) In the sodium-based ether electrolyte (BE2: 1M $NaPF_6$ DGM), our optimized strategy results in an improved anodic stability limit from 5.0 V to 5.3 V when the DFOB concentration is set at 0.2M.

(c) For carbonate-based sodium ion batteries (BE3: 1M $NaPF_6$ EC/DEC), we employ a slightly higher

DFOB concentration of 0.3M, and observe a more pronounced enhancement in anodic stability, with the limit rising from 4.8 V to 5.3 V.

These results conclusively demonstrate that our dual-domain molecular-locked strategy achieves consistent and significant improvements in anodic stability across diverse battery systems and electrolyte formulations.

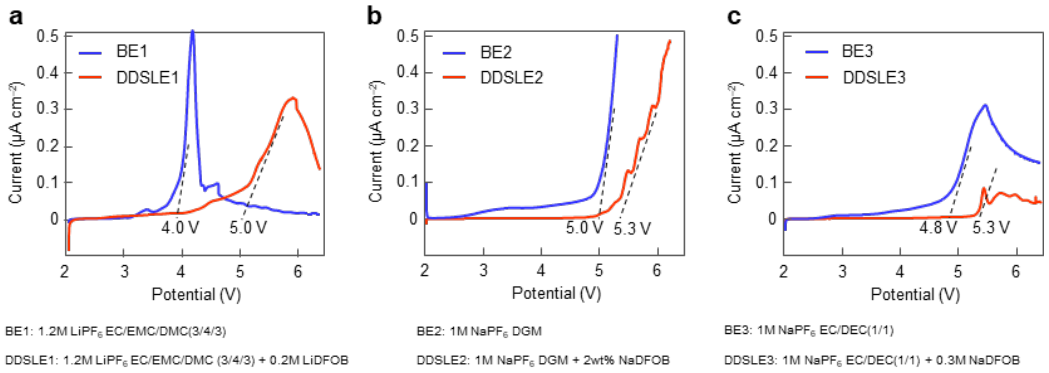

Figure R8. LSV curves in metal||steel sheet cells. (a) Li||steel sheet cells with BE1 and DDSLE1 electrolytes. (b) Na||steel sheet cells with BE2 and DDSLE2 electrolytes. (c) Na||steel sheet cells with BE3 and DDSLE3 electrolytes.

On page 8 of revised manuscript, we have added the discussion with "Furthermore, the dual-domain molecular-locked strategy demonstrates broad applicability across various battery systems, achieving markedly elevated anodic stability limits in diverse electrolyte formulations (Supplementary Fig. 25).".

On page 26 of revised Supplementary information, we added the Figure R8 as Supplementary Fig. 25.

Question 3. The authors correlate the electron tunneling probability of the CEI with the bandgap of its components. However, the underlying physical mechanism linking bandgap to tunneling probability, specifically concerning electronic transitions, remains incompletely elucidated.

Answer: We appreciate the reviewer's professional suggestion. As advised, we have elaborated on the correlation between electron tunneling probability across the CEI and the bandgap of its components by considering the electronic structure and quantum tunneling behavior at interface.

As illustrated in **Figure R9a**, the CEI acts as an electron-passivating layer between cathode and electrolyte. The bandgap E_g (CEI) of the CEI's component fundamentally determines the electronic barrier properties, which in turn influence the electron tunneling probability. Electron tunneling through the CEI follows quantum mechanical principles, where the transmission probability decreases exponentially with both the height and the width of the potential barrier.

The bandgap directly governs the barrier height: a larger E_g corresponds to a higher energy barrier, which strongly suppresses electron tunneling, while a smaller E_g reduces the barrier and promotes tunneling. Additionally, the bandgap affects the availability of electronic states within the CEI that can participate in tunneling. Materials with a large bandgap provide fewer accessible states within the relevant energy range, further limiting tunneling probability. In contrast, materials with a smaller bandgap offer more accessible states, facilitating electron transfer via direct or trap-assisted tunneling mechanisms.

In battery operation, CEI components with an appropriately large bandgap can effectively block

electron leakage from cathode to electrolyte, thereby mitigating parasitic reduction reactions and enhancing interfacial stability (**Figure R9b**). This electronic passivation is crucial to suppress continuous electrolyte decomposition and CEI growth, ultimately improving cycling stability. For instance, in this study, boride/fluorides with bandgaps exceeding 6.2 eV are demonstrated to effectively inhibit electron tunneling above 4.0 V, thereby reducing current leakage and persistent interfacial side reactions.

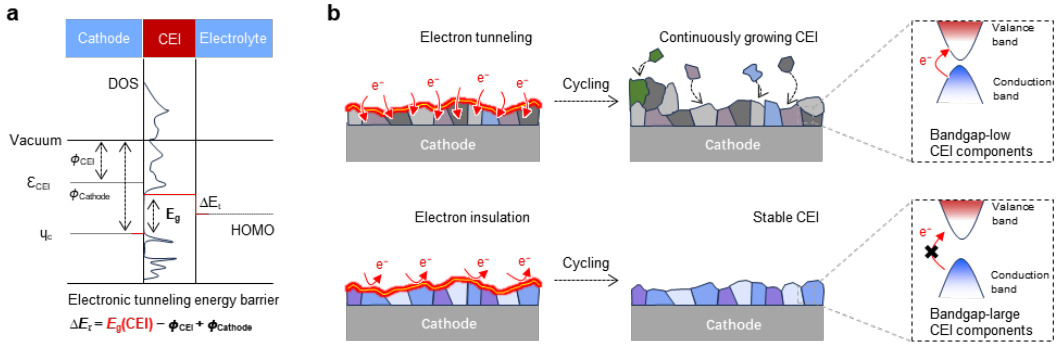

Figure R9. Schematic illustration of the CEI as an electronic passivation layer. (a) Structure and band alignment of the CEI. (b) Electron tunneling behavior across the CEI.

On page 5 of revised manuscript, we have revised the discussion with "The electronic origin of anion-derived insoluble enhancing the antioxidation stability at cathode/electrolyte interface was rigorously evaluated through integrated theoretical and experimental analysis, with electron tunneling resistance identified as the primary determinant for electrochemical stability at high voltage (Supplementary Fig. 12).".

On page 13 of revised Supplementary information, we added the Figure R9 as Supplementary Fig. 12.

On page 36 of revised Supplementary information, we added the discussion as Supplementary note 4.

Question 4. A significant overcharge phenomenon is observed in the mass spectrometry experiment using the baseline electrolyte (Fig. 2g). However, the electrochemical testing in coin cell (Fig. 6g) shows a less pronounced overcharge effect, allowing for cycling beyond 50 cycles. Please clarify this apparent discrepancy in detail.

Answer: Thank you for this insightful and detailed question. The observed difference in the overcharge phenomenon between *in situ* differential electrochemical mass spectrometry (*in situ* DEMS) test and coin-cell cycling primarily stems from fundamental differences in cell configuration (**Figure R10**) and operational conditions of two tests.

(1) Key structural and operational differences

The observed discrepancy stems from fundamental distinctions between the two testing platforms, which establish vastly different interfacial and kinetic conditions for the same electrochemical reactions.

(a) Divergent design objectives and resulting structure

In situ DEMS cell: engineered primarily for real-time gas analysis, its structure prioritizes gas transport over electrochemical interface quality. It employs a porous Al mesh current collector (*vs.* conventional foil) and features a grooved cathode column with a central vent to channel gases to the spectrometer. This design inherently compromises the intimacy and uniformity of electrode/electrolyte

contact.

Coin cell: as a standard electrochemical testing platform, it is optimized for consistent electrical contact. It uses flat, dense current collectors and is sealed under high, uniform pressure, promoting a stable and homogeneous interface.

(b) Assembly process and interface quality

In situ DEMS cell: uses a custom, reusable mold assembled manually. This process results in less uniform stack pressure distribution and greater variability, leading to a non-ideal, high-impedance interface prone to localized current hotspots.

Coin cell: assembled using automated commercial equipment with precise, high-pressure crimping. This ensures reproducible and uniform interfacial contact, minimizing initial impedance and promoting even current distribution.

(c) Operational environment and reaction kinetics

In situ DEMS cell: operates under a continuous argon purge, creating an open, dynamic system. Gaseous reaction products are immediately removed from the cell.

Coin cell: a hermetically sealed, static system. All gaseous and soluble reaction products accumulate within the confined cell volume, altering the local chemical environment.

These structural and operational differences collectively explain why the *in situ* DEMS test, while excellent for diagnosing failure mechanisms, presents a more accelerated and severe degradation profile compared to a standard coin cell test.

(2) Analysis of the discrepancy in overcharge behavior

The more pronounced overcharge observed in *in situ* DEMS test is attributed to the combined effects of inferior interface stability and an operational environment that kinetically promotes parasitic reactions.

(a) Accelerated interface degradation in *in situ* DEMS cell

Non-ideal interface contact: the grooved current collector and manual assembly of *in situ* DEMS cell result in less uniform pressure distribution at cathode interface compared to standard coin cells. This leads to inhomogeneous current distribution, localized high impedance, and exacerbated side reactions.

Consequence: a defective CEI forms more readily and is less effective. The increased and unstable interfacial impedance directly contributes to the severe overcharge phenomenon, as a greater fraction of the charging time/energy is consumed by parasitic processes rather than useful Na^+ intercalation.

(b) Kinetic promotion of parasitic reactions in *in situ* DEMS cell

Product removal shifts reaction equilibrium: in *in situ* DEMS cell, the constant Ar flow immediately removes gaseous decomposition products (e.g., CO_2, C_2H_6). According to Le Chatelier's principle, this continuous product removal shifts the equilibrium of electrolyte decomposition reactions forward, promoting their continuous progression.

Contrast in coin cells: in a sealed coin cell, these gaseous products accumulate, increasing their partial pressure and thereby thermodynamically suppressing further decomposition. This natural self-inhibition moderates the rate of parasitic reactions and mitigates the overcharge effect over cycles.

In summary, the apparent discrepancy stems from the operational conditions of the *in situ* DEMS cell. Although excellent for operando gas analysis, its poor interfacial contact and product removal inadvertently accentuate the failure mechanisms of the unstable baseline electrolyte. The standard coin cell, with its more robust interface and sealed environment, provides a degree of inherent kinetic stabilization, allowing for more extended cycling despite the electrolyte's intrinsic instability. This comparison effectively highlights how cell design and testing conditions can significantly influence the observed degradation kinetics.

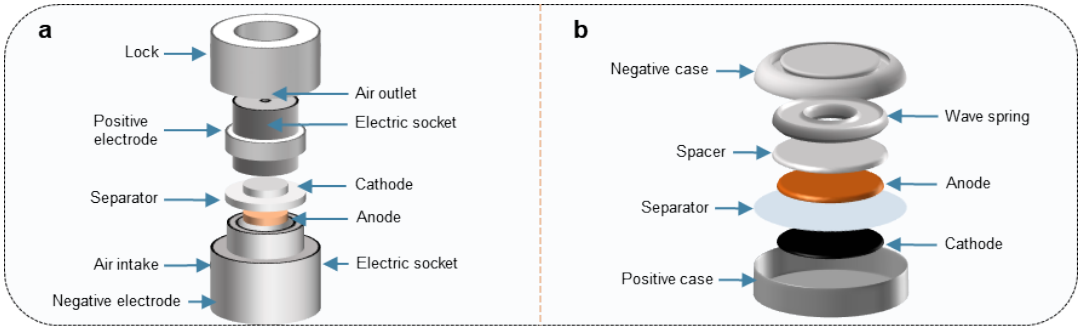

Figure R10. Schematic illustrations of the two test cell configurations. (a) Custom cell for *in situ* DEMS cell. (b) Standard coin cell.

On page 4 of revised manuscript, we have updated the discussion into "*In situ* differential electrochemical mass spectrometry (*In situ* DEMS) further corroborates the analysis from the perspective of gas evolution. For DDSLE-involved cells, CO_2 evolution initiates at 2.9 V (charging), intensifies by 3.9 V, dips then rise again above 4.3 V, with minimal CO/CH_4 (Fig. 2g). This confirms $DFOB^-$ decomposition (2.9–4.3 V) as the primary CO_2 source before solvent decomposition (>4.3 V).[23] BE-involved cells display earlier CO_2 onset (2.7 V) and recurring CO_2/CO peaks at 3.7 V (discharge) due to unshielded interface structures. The more pronounced overcharge phenomenon can be attributed to inherent structural instabilities combined with harsh operating conditions of *in situ* DEMS cell, which collectively result in degraded interfacial properties and poor kinetic behaviors (Supplementary Fig. 10 and note 3).".

On page 11 of revised Supporting Information, we have added the Figure R10 as Supplementary figure 10.

On page 34−35 of revised Supporting Information, we have added the discussion as Supplementary note 3.

Question 5. The data points in Figure 6b representing comparative performance lack clear sourcing and context. Adding a supplementary table listing the corresponding references and key parameters (e.g., cycle lifetime, charging rate, specific electrolyte used) for each data would significantly improve clarity.

Answer: Thanks for your careful review and valuable suggestions. We have compiled the data points in Figure 6b along with their corresponding information into a table (Table R1). This includes the cathode, anode, electrolyte, rate (based on 1C = 100 mA/g), cycle number, and the decay rate per cycle, in order to present the information more clearly.

Table R1. Comparison of Na||NFS cells based on DDSEL electrolyte with other reported SIBs.

Cathode	Anode	Electrolyte	Decay rate per cycle	Cycle number/rate	Cut-off voltage	Ref.
$Na_{2.26}Fe_{1.87}(SO_4)_3$	**Na**	**1M $NaPF_6$ + 0.4M NaDFOB in EC/EMC**	**$7.15*10^{-4}$**	**16500/5C**	**4.5 V**	**This work**
$Na_{2.4}Fe_{1.8}(SO_4)_3$	Na	1M $NaClO_4$ in EC/DEC	0.0042	10000/10C	4.5 V	*J. Energy Chem.* **2021**, 54, 564
$Na_{2.4}Fe_{1.8}(SO_4)_3$	$NaTi_2(PO_4)_3$	1M $NaClO_4$ in EC/PC + 5% FEC	0.00293	10000/10C	4.5 V	*Adv. Funct. Mater.* **2024**, 35, 2411007
$Na_{6-2x}Fe_x(SO_4)_3$	Na	1M $NaClO_4$ in EC/DEC + 5% FEC	0.00276	10000/30C	4.5 V	*Science Bulletin* **2023**, 68, 1894

$Na_{2.5}Fe_2(SO_4)_{2.5}(PO_4)_{0.5}$	Na	1M $NaClO_4$ in EC/DEC + 5% FEC	0.00112	10000/10C	4.5 V	*J. Am. Chem. Soc.* **2025**, 147, 14635−14646
$Na_{2.9}Fe_{1.7}(SO_4)_{2.7}(PO_4)_{0.3}$	Na	1M $NaClO_4$ in EC/DEC + 5% FEC	0.00395	6000/30C	4.5 V	*Nano Energy* **2024**, 125, 109557
$Na_2Fe(SO_4)_2$	Na	1M $NaPF_6$ in EC: DMC	0.00231	3500/3C	4.5 V	*Energy Storage Mater.* **2025**, 74, 103882
$Na_{2.26}Fe_{1.87}(SO_4)_3$	Na	1M $NaClO_4$ in EC/PC + 5% FEC	0.00608	5700/5C	4.5 V	*Nat. Commun.* **2023**, 14, 3701
$Na_{2.466}Fe_{1.724}Mg_{0.043}(SO_4)_3$	Na	1M $NaClO_4$ in EC/PC + 5% FEC	0.00584	5000/5C	4.5 V	*eScience*, **2025**, 5, 100313
$Na_6Fe_5(SO_4)_8$	Na	1M $NaClO_4$ in PC	0.001	1000/2C	4.5 V	*J. Mater. Chem. A* **2019**, 7, 14656
$Na_4Fe_3(PO_4)_2(P_2O_7)$	Na	1M $NaClO_4$ in PC + 5% FEC	0.0014	5000/20C	4.1 V	*Angew. Chem. Int. Ed.* **2025**, 64, e20250269
$Na_4Fe_3(PO_4)_2(P_2O_7)$	Na	1M $NaClO_4$ in EC/PC + 5% FEC	0.00286	10000/50C	4.3 V	*J. Am. Chem. Soc.* **2025**, 147, 16, 13905
$Na_3V_2(PO_4)_3$	Na	EC/PC/EP-NaDFOB/SN	0.00204	7000/5C	3.9 V	*Angew. Chem. Int. Ed.* **2024**, 63, e202401051
$Na_3V_2(PO_4)_3$	Na	1M $NaPF_6$ in diglyme	0.00345	2000/50C	4.2 V	*ACS Nano* **2024**, 18, 9354–9364
$Na_{3.6}VMn_{0.4}Fe_{0.4}Ti_{0.1}Zr_{0.1}(PO_4)_3$	Na	1M $NaClO_4$ in EC/DEC + 5% FEC	0.00194	10000/10C	3.8 V	*Adv. Energy Mater.* **2025**, 15, 2500502
$Na_3V_2(PO_4)_3$	Na	0.75M $NaClO_4$ FEC/PC + 0.01M LiTFSI	0.00108	10000/60C	3.8 V	*J. Am. Chem. Soc.* **2023**, 145, 21661
$Na_{0.67}Fe_{0.3}Mn_{0.7}O_2$	Na	1M $NaClO_4$ in PC + 5% FEC	0.058	300/2C	4.2 V	*Adv. Funct. Mater.* **2025**, 35, 2504354
$Na_{0.44}Mn_{0.85}Ti_{0.15}O_2$	Na	1M $NaClO_4$ in EC/DEC + 5% FEC	0.02231	650/2C	4.0 V	*Adv. Mater.* **2024**, 36, 2407994
$Na_{0.75}Li_{0.25}Mn_{0.75}O_2$	Na	1M $NaClO_4$ in PC + 5% FEC	0.0876	100/0.2C	4.4 V	*Energy Environ. Sci.* **2025**, 18, 7995–8008
$Na_{0.61}Ca_{0.05}[Li_{0.1}Ni_{0.23}Mn_{0.67}]O_{1.95}F_{0.05}$	Na	1M $NaClO_4$ in EC/DEC	0.01818	1100/16C	4.3 V	*Adv. Mater.* **2024**, 36, 2407519
$NaNi_{0.3}Cu_{0.1}Fe_{0.2}Mn_{0.3}Ti_{0.1}O_2$	Na	1M $NaClO_4$ in EC/DEC/DMC	0.03	500/1C	4.0 V	*Nat. Energy* **2024**, 9, 1529–1539
$Na_{0.8}Cu_{0.22}Li_{0.08}Mn_{0.67}O_2$	Na	1M $NaClO_4$ in PC + 5% FEC	0.036	500/10C	4.4 V	*J. Am. Chem. Soc.* **2023**, 145, 22708
O3-$Na_{0.8}Li_{0.2}Fe_{0.2}Ru_{0.6}O_2$	Na	1M $NaClO_4$ in EC/PC + 5% FEC	0.046	100/1C	4.5 V	*J. Am. Chem. Soc.* **2024**, 146, 13924
$Na_{2-x}Mn_{0.8}Fe_{0.2}[Fe(CN)_6]_y \cdot nH_2O$	Na	1M $NaClO_4$ in EC/DEC + 5% FEC	0.0406	500/1C	4.0 V	*ACS Nano* **2025**, 19, 22093
Prussian blue	Na	1M $NaClO_4$ in EC/DEC + 5% FEC	0.00525	4000/20C	4.1 V	*Angew. Chem. Int. Ed.* **2025**, 64, e202421916
$Na_{1.34}Ni[Fe(CN)_6]$	Na	1M $NaClO_4$ in EC/DEC + 5% FEC	0.00269	13000/5C	4.2 V	*Small* **2025**, 21, 2407570
FeHCF-P	Na	1M $NaClO_4$ in EC/DEC + 5% FEC	0.034	500/1C	4.1 V	*Nano-Micro Lett.* **2022**, 14, 9
$Na_{1.76}FeFe(CN)_6 \cdot 2.6H_2O$	Na	1M $NaClO_4$ in EC/PC + 3% FEC	0.00875	2000/5C	3.8 V	*Adv. Funct. Mater.* **2022**, 32, 2111727

$Na_2Mn_{0.2}Fe_{0.2}Co_{0.2}Ni_{0.2}Cu_{0.2}[Fe(CN)_6]$	Na	1M $NaClO_4$ in EC/DEC + 5% FEC	0.00393	9000/5C	4.2 V	*Angew. Chem. Int. Ed.* **2025**, 64, e20251289

On page 7−8 of revised manuscript, we have updated the discussion with "Remarkably, at 10C over 16,500 cycles, DDSLE-involved cell achieved 88.2% capacity retention with an average CE of 99.9%. This performance sets a new benchmark for cycle life and degradation rate in high-voltage NFS cathodes operating to 4.5 V (Fig. 6b, Supplementary table 3). Even when compared to batteries using other cathode materials, such as polyanionic compounds (PACs), Prussian blue analogues (PBAs), and transition metal oxides (TMOs), which typically operate at lower voltages (3.8–4.3 V), the DDSLE-based Na||NFS cell still demonstrates remarkable cycling stability.".

On page 28−29 of revised Supporting Information, we have added the Table R1 as Supplementary table 3.

Question 6. While the supporting information is detailed, error bars or statistical analysis are absent for critical metrics including ionic conductivity, transference number, and oxidation window. Providing reproducibility data and uncertainty analysis is essential to strengthen scientific reliability. Furthermore, it remains unclear whether the enhanced oxidation stability extends to alternative substrates used as the working electrode instead of steel sheet.

Answer: Thanks for your valuable suggestion. We fully agree with the necessity of providing statistical data. We have provided supplementary details for all key performance metrics (including ionic conductivity, transference number, and oxidation window). Furthermore, we expand the substrates used in oxidation stability tests. Related result and analysis are summarized as follows:

(1) Regarding data reproducibility and error analysis

The number of replicates for all experiments (at least three independent trials) and present the complete error bars along with specific values in the form of "mean ± standard deviation" within the main text or the supporting information figures/tables.

(a) Ionic conductivity. EIS spectra from three symmetric stain steel cells were measured (**Figure R11**). The error for all tested electrolytes fell within ±0.20 mS cm^{-1}. The specific values are as follows:

Baseline electrolyte (BE, 1M $NaPF_6$ in EC/EMC): 2.56 ± 0.19 mS cm^{-1}

BE + 0.2M NaDFOB: 1.73 ± 0.07 mS cm^{-1}

BE + 0.4M NaDFOB: 2.10 ± 0.10 mS cm^{-1}

BE + 0.6M NaDFOB: 1.47 ± 0.04 mS cm^{-1}

BE + 0.8M NaDFOB: 1.98 ± 0.05 mS cm^{-1}

BE + 1.0M NaDFOB: 2.04 ± 0.02 mS cm^{-1}

These small deviations across multiple replicates demonstrate the reliability and consistency of our conductivity measurements.

(b) Na^+ transference number. Chronoamperometry data from three symmetric Na||Na cells were measured (**Figure R12**), demonstrating a higher Na^+ transference number (0.474±0.048) in DDSLE electrolytes compared to the BE electrolyte (0.391±0.004).

(c) Anodic stability limit. LSV measurements performed on three Na||stainless steel cells demonstrate that the anodic stability limit of BE electrolytes ranges from 3.4 V to 3.7 V, whereas that of DDSLE electrolytes reaches 5.0 V to 5.1 V (**Figure R13**). These results clearly confirm that the dual-domain molecular-locked design effectively enhances the anodic stability of the electrolyte.

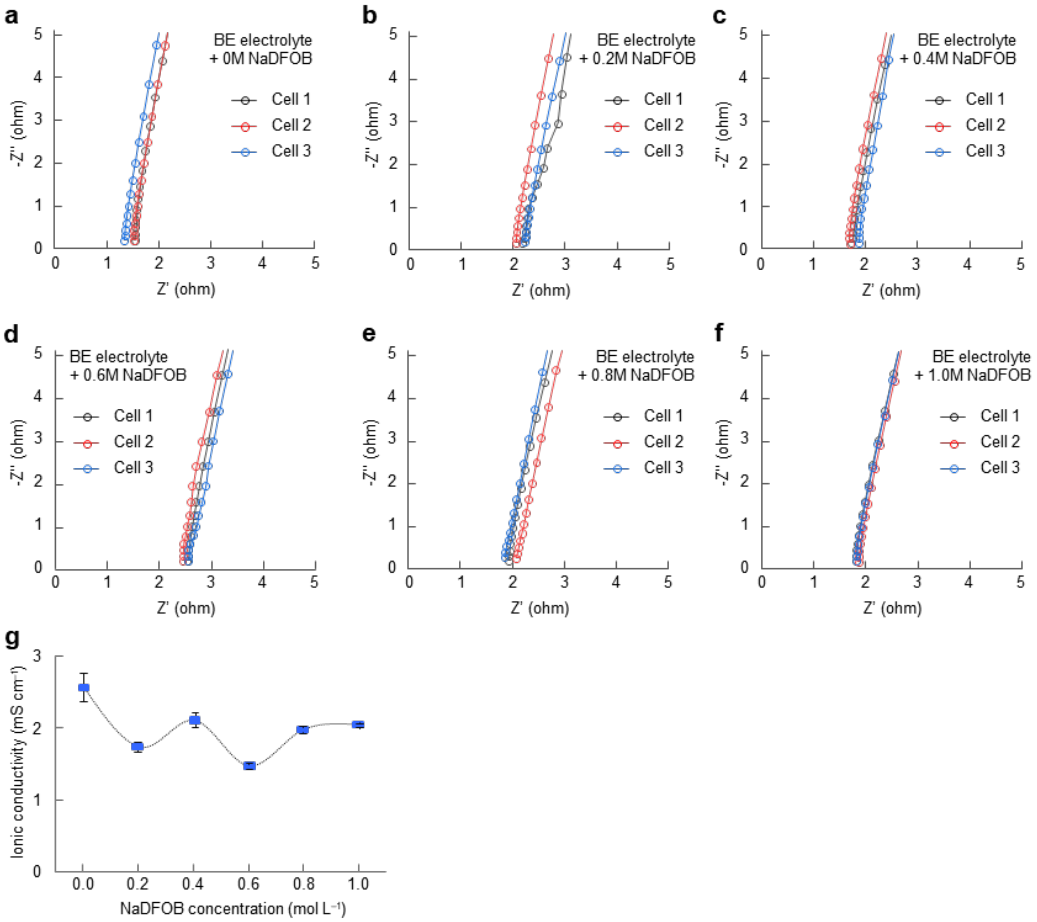

Figure R11. EIS plots in steel sheet||steel sheet cells for BE electrolytes with different DFOB concentrations. (a) 0M. (b) 0.2M. (c) 0.4M. (d) 0.6M. (e) 0.8M. (f) 1.0M. (g) Ionic conductivities with error bar based three parallel data.

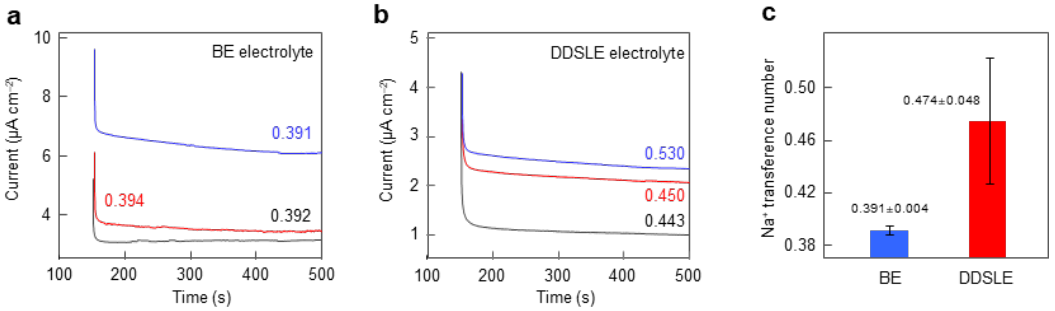

Figure R12. Chronoamperometry profiles in three Na||Na symmetric cells. (a) BE electrolyte. (b) DDSLE electrolyte. (c) Calculated Na^+ transference number with error bar.

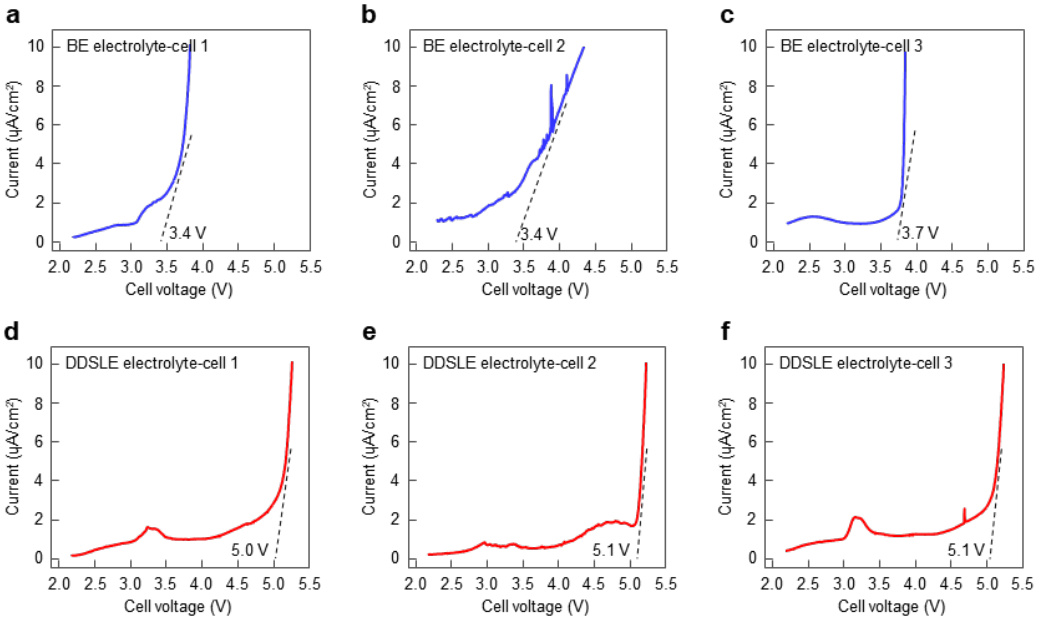

Figure R13. LSV curves in Na Na||steel sheet cells. (a–c) BE electrolyte. (d–f) DDSLE electrolyte.

(2) Regarding the oxidation stability on different substrates

To verify whether the improved oxidation stability is generally applicable across different current collectors, supplemental tests were conducted using Ni foil. LSV tests were conducted under identical conditions (scan rate: 0.2 mV/s). The results show that the anodic stability limit in DDSLE electrolyte is also significantly enhanced on Ni foil, reaching a potential of 5.0 V (**Figure R14**). This increase in oxidation potential is comparable to that observed with the stainless-steel current collector (approximately 1.7 V *vs.* 1.8 V relative to their respective baseline systems).

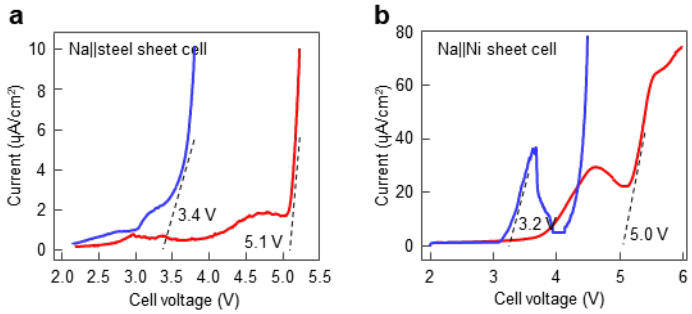

Figure R14. LSV curves of DDSLE electrolyte in different cells. (a) Na||steel sheet cells. (b) Na||Ni sheet cells.

On page 3 of revised manuscript, we have revised the discussion into "While BE electrolyte offers favorable ionic conductivity, low viscosity, and separator wettability, it exhibits poor high-voltage stability (~3.4 V *vs.* Na^+/Na).[11] Introducing low-concentration NaDFOB slightly reduced conductivity due to its lower intrinsic conductivity versus $NaPF_6$, hindered ion migration, and increased viscosity (Fig. 1a and Supplementary Figs. 1–2). Importantly, at this concentration (0.2M), NaDFOB addition fails to satisfactorily enhance the electrolyte's anodic stability limit, primarily because it cannot sufficiently control the structure within the bulk electrolyte and at the cathode interface (Supplementary note 1). Higher NaDFOB concentrations modestly recovered conductivity and further increased viscosity, but

beyond 0.6M, electrolyte cloudiness indicated salt precipitation. Thus, 0.4M NaDFOB was selected as optimal for the DDSLE electrolyte (1M $NaPF_6$ + 0.4M NaDFOB in EC/EMC).".

On page 3 of revised manuscript, we have revised the discussion into "Moreover, the compacted solvation cluster decreased the hydrodynamic radius, increasing the Na^+ transference number from 0.391±0.004 to 0.474±0.048 (Fig. 1i and Supplementary Fig. 7).".

On page 5 of revised manuscript, we have added the discussion with "The preferential oxidation of $DFOB^-$, indicated by minor current peaks at 3.0–3.4 V, elevates the anodic stability limit of electrolytes from 3.4 V (BE electrolyte) to 5.1 V (DDSLE electrolyte, Fig. 3a). This enhanced oxidative stability is further confirmed through statistical data and tests on additional substrate (Ni foil) in Na||inert metal coin cells (Supplementary Fig. 11).".

On page 15 of revised manuscript, we have added the Figure R11 into Figure 1a.

On page 2 of revised Supporting Information, we have added Figure R11 as Supplementary Fig. 1.

On page 8 of revised Supporting Information, we have added Figure R12 as Supplementary Fig. 7.

On page 12 of revised Supporting Information, we have added Figures R13−14 as Supplementary Fig. 11.

Question 7. Experimental details:

a. A more detailed description of how the cathode–electrolyte composite model was constructed and the kinetic optimization procedures applied.

b. The scan rates used in LSV, *in situ* characterizations, and other electrochemical tests should be specified.

c. Detailed procedures for XRD testing and refinement should be described.

d. The caption for Supplementary Figure 3 is currently missing and needs to be provided.

Answer: We sincerely appreciate the reviewer's thorough feedback regarding experimental documentation. The following revisions have been implemented.

(a) For the cathode-electrolyte composite model construction and kinetic optimization, molecular dynamics (MD) simulations were performed using a conventional unit cell of $Na_{2.26}Fe_{1.87}(SO_4)_3$ exposing the (200) crystal plane. Simulations employed γ-centered k-point sampling with a 450 eV plane-wave energy cutoff, achieving total energy convergence to 10^{-5} eV. The DFT-relaxed structure was thermally equilibrated in the NVT ensemble using a 0.5-fs timestep (corrected from 0.05 fs) and a Nosé-Hoover thermostat (Nosé-mass parameter: 1000 timesteps), with stepwise heating from 100 K to the target temperature of 300 K.

(b) Electrochemical test parameters are specified as follows: LSV measurements used a uniform scan rate of 0.2 mV/s. *In situ* Raman spectroscopy and mass spectrometry data were collected during galvanostatic cycling at 50 μA cm^{-2}. *In situ* EQCM employed a constant potential increment mode at 50 mV/s (2.0–4.5 V *vs.* Na^+/Na, 100 cycles). Galvanostatic charge-discharge tests (Na||NVP, Na||P2-TMO, Na||NFS) were conducted at 1C rate using both DDSLE and baseline electrolytes (1C= 100 mA g^{-1}).

(c) *Ex situ* XRD characterization was performed on a Bruker D8 ADVANCE diffractometer (Cu Kα radiation, λ = 1.54056 Å) with a scan rate of 1 ° min^{-1}. Rietveld refinement was executed using GSAS-II software.

(d) We apologize for this oversight. The caption has been added in Supplementary Figure 3.

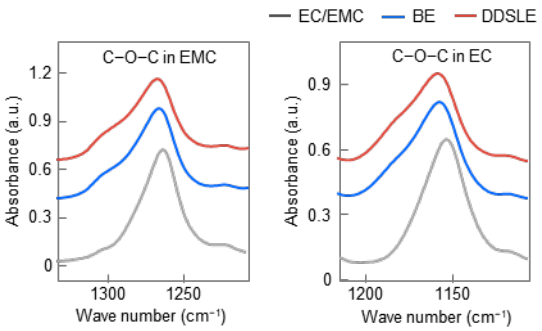

Figure R15. FTIR spectra tracking salt dissolution in EC/EMC from the BE to the DDSLE electrolytes.

On page 10−11 of revised manuscript, we have added the description in *in situ* characterizations with "During discharge process at 50 μA cm^{-2}, evolved gaseous species were routed through a cryogenic condenser to trap electrolyte volatiles prior to detection by the HPR-20 DEMS system (Hiden Analytical). The sensor coated with Au film acted as a working electrode, and charge-discharge process employed a constant potential increment mode at 50 mV/s (2.0–4.5 V *vs.* Na^+/Na, 100 cycles). The charge/discharge process was carried out on a Lvium electrochemical workstation with a current density of 50 μA cm^{-2}."

On page 11 of revised manuscript, we have added the description in materials characterizations with "Synchrotron high-pressure powder XRD was carried out at Dr. Tadich Anton and Dr. Thomson Lars from ANSTO Australia using X-rays with a wavelength of 0.6887 Å, and GSAS-II software conducted Rietveld refinement."

On page 11 of revised manuscript, we have added the description in computational details with "For the cathode-electrolyte composite model construction and kinetic optimization, MD simulations were performed using a conventional unit cell of $Na_{2.26}Fe_{1.87}(SO_4)_3$ exposing the (200) crystal plane. Simulations employed γ-centered k-point sampling with a 450 eV plane-wave energy cutoff, achieving total energy convergence to 10^{-5} eV. The DFT-relaxed structure was thermally equilibrated in the NVT ensemble using a 0.5-fs timestep (corrected from 0.05 fs) and a Nosé-Hoover thermostat (Nosé-mass parameter: 1000 timesteps), with stepwise heating from 100 K to the target temperature of 300 K."

On page 5 of revised Supporting Information, we have updated Supplementary Figure 3.

All changes are marked in yellow in the revised manuscript for reference.

Response to Reviewer 3:

The manuscript reports a NaDFOB/$NaPF_6$-based carbonate electrolyte that enables high-voltage, long-life sodium metal batteries. This electrolyte shows excellent electrochemical properties and can stabilize both the SEI on Na metal and the CEI on a 4.5 V cathode. The working mechanism is systematically investigated through experimental analyses and theoretical calculations. These findings provide an important reference for designing electrolytes suitable for high-voltage sodium batteries. The revision comments are as follows.

Answer: We thank the reviewer for their thorough review and positive evaluation of our work. We have carefully refined and polished the details and expressions in the revised manuscript to ensure it meets the journal's publication standards.

Question 1. The meanings of "dual-domain" and "solvent-locked" are not clearly explained. Please clarify where the "dual domains" are in the NaDFOB–$NaPF_6$ electrolyte, and how the solvent is "locked."

Answer: Sorry for our unclear description. We further clarified the meanings of "dual-domain" and "solvent-locked", and solvent-locked mechanism in DDSLE electrolyte, as detailed below.

(1) Dual-domain clarification

The term "dual-domain" refers to the two distinct spatial and functional regions within the NaDFOB–$NaPF_6$ electrolyte system, where the $DFOB^-$ anion provides targeted stabilization:

Domain I (bulk electrolyte phase): in bulk solution, $DFOB^-$ anions, due to their large steric hindrance and intrinsically weak solvation strength towards Na^+, remain excluded from the primary solvation shell. Instead, they reside at the outer periphery of the solvated Na^+ structure. This positioning creates a steric crowding effect, exerting compressive force on the inner solvation shell.

Domain II (cathode/electrolyte interface): at the interface with the high-voltage NFS cathode, $DFOB^-$ anions exhibit preferential adsorption over PF_6^- anions and solvent molecules (EC, EMC). This leads to the formation of a dense, anion-rich interfacial shield directly on cathode surface.

(2) Solvent-locked clarification and mechanism

The term "solvent-locked" precisely describes the dual-action mechanism that secures solvent molecules against oxidative degradation:

Locking in bulk electrolyte phase (domain I): the steric crowding by $DFOB^-$ anions in the bulk electrolyte mechanically constrains the solvation shell. This compression strengthens the coordination bonds between inner-shell carbonate solvents (e.g., EC, EMC) and central Na^+ ion. This enhanced binding effectively "locks" these solvent molecules into a more stable configuration without covalent bonding, primarily through steric enforcement.

Locking out at cathode/electrolyte interface (domain II): while the bulk mechanism locks coordinated solvents, residual free solvent molecules inevitably present in electrolyte pose a separate risk. The $DFOB^-$-derived interfacial shield formed in domain II physically blocks access of these free solvents to the highly oxidizing cathode surface, preventing their direct contact and decomposition.

This "dual-domain solvent-locked" strategy resolve the persistent instability challenge of industrial $NaPF_6$/carbonate-based electrolytes at high voltage, by restricting the freedom degrees and reactivity of solvent molecules.

On page 2 of revised manuscript, we have updated the discussion into "The symmetric difluoro(oxalato)borate anion ($DFOB^-$), employed as an additive to the industrial electrolyte (1M $NaPF_6$ in EC/EMC), exhibits weak coordination with carbonate solvents but strong binding affinity towards Na^+-exposed cathode surface. Leveraging steric hindrance and electron-withdrawing effects of $DFOB^-$

anion, the tailored electrolyte achieves effective locking to solvent molecules at dual domains of bulk-phase electrolyte (domain I) and cathode interface (domain II). We therefore designate it as a dual-domain solvent-locked electrolyte (DDSLE)."

On page 9 of revised manuscript, we have updated the conclusion content into "By integrating a symmetrical difluoro(oxalato)borate anion ($DFOB^-$), a solvent-reinforced Na^+ solvation within bulk solution (domain I) and an anion-rich shield at cathode interface (domain II) are constructed, effectively restricting the freedom degrees and reactivity of solvent molecules. We called it, therefore, as dual-domain solvent-locked electrolyte."

Question 2. For Na-metal coin cells, why was a glass-fiber membrane used instead of conventional PP separators? In contrast, the pouch cells use a PP separator.

Answer: We sincerely appreciate the reviewer's insightful comments. This is a highly professional and important question, as it touches upon the key differences between fundamental laboratory research and practical application testing. In sodium-ion battery (SIB) research, the choice of separators for coin cells versus pouch cells is driven by their differing objectives, testing conditions, and associated requirements. The detailed reason is as follows.

(1) Reasons for use of glass fiber separator in coin cells

Coin cells are designed for precise evaluation of fundamental electrochemical performance, with the primary goal of minimizing interference to accurately characterize the intrinsic properties of materials and electrolytes.

(a) Ensuring sufficient wetting and a stable interface. The glass fiber separator exhibits extremely high porosity (pore size 0.6–2.7 μm) and excellent wettability (as demonstrated in **Figure R2**), enabling rapid, thorough absorption of a large volume of electrolyte. This is critical for maintaining a consistently wetted interface with electrodes, preventing localized dry-out, and thus yielding stable, reproducible electrochemical signals (e.g., overpotential, Coulombic efficiency).

(b) Providing mechanical support and uniform current distribution. Rigid structure in glass fiber separator can effectively resist puncture during sodium deposition/stripping. The greater thickness also helps homogenize Na^+ flux, suppressing localized, rapid dendrite growth.

(c) Tolerance to highly reactive environments. Composed primarily of SiO_2, glass fiber demonstrates excellent chemical and electrochemical inertness. It withstands the harsh conditions at the sodium metal anode and high-voltage cathode without participating in side reactions, ensuring test results reflect the true performance of the electrode materials.

(2) Reasons for use of PP separator in pouch cells

Pouch cells are engineered to simulate devices closer to practical application, requiring a design that balances performance, safety, cost, and manufacturability.

(a) Thickness and energy density. Commercial polyolefin (PP) separators are very thin (typically <60 μm), significantly reducing the volume and weight of inactive components and thereby enhancing the overall battery energy density—an advantage unmatched by much thicker glass fiber separators (typically >300 μm).

(b) Cost and manufacturing maturity. PP separators are low-cost and fully compatible with established large-scale roll-to-roll manufacturing processes for lithium-ion batteries, making them the standard for industrial applications. In our lab-scale procurement, the PP separator costs only ~10 RMB per meter (100 mm width), whereas the glass fiber separator for the same area costs ~380 RMB per meter. For pouch cells assembly requiring multiple trials, the cost difference is significant and decisive.

(c) Practical application conditions. In pouch cells, the electrolyte amount is optimized (not excessive), and assembly processes ensure adequate wetting of the PP separator. When the electrolyte formulation itself, such as the DDSLE in this work, can provide excellent interfacial wetting and compatibility, the long-term cycling risks associated with using thin PP separators are substantially mitigated.

In summary, this difference reflects the distinct requirements of the research and application processes. Coin cells with glass fiber separators serve as a precise scientific platform to reveal mechanisms and validate material potential under idealized, stable conditions. In contrast, pouch cells with PP separators act as a product prototype to validate technological feasibility under near-practical conditions.

Question 3. How does adding NaDFOB affect the electrolyte viscosity? Please show the viscosity data of the electrolytes listed in Figure 1a.

Answer: Thanks for your valuable comments. As suggested, we further measured the viscosities of electrolytes with varying concentrations of NaDFOB. All tests were repeated three times to ensure statistical significance of the data.

The results show that the baseline electrolyte exhibited a viscosity of 3.34±0.26 mPa·s (**Figure R16**). As the concentration of NaDFOB increased, the viscosity of the electrolyte gradually rose: at concentrations of 0.2M and 0.4M, the viscosities reached 4.10±0.06 mPa·s and 5.01±0.03 mPa·s, respectively. Upon further increasing the salt concentration, even when insoluble substances appeared, the viscosity continued to increase, reaching 5.61±0.05 mPa·s at 0.6 M, 6.19±0.10 mPa·s at 0.8 M, and 7.06±0.03 mPa·s at 1.0 M.

These findings indicate that the addition of NaDFOB significantly increases the viscosity of the electrolyte, and this effect intensifies with higher concentrations, maintaining an upward trend even after supersaturation occurs.

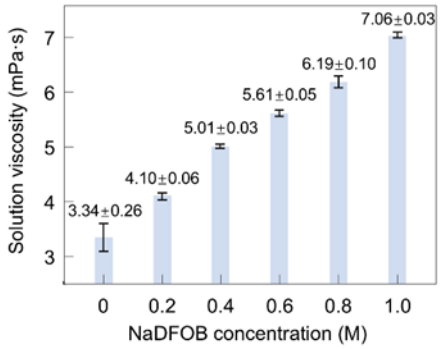

Figure R16. Effect of NaDFOB concentration on the viscosity of the baseline electrolyte (1M $NaPF_6$ in EC/EMC). Error bars are calculated based on three independent experiments.

On page 3 of revised manuscript, we have revised the discussion with "While BE electrolyte offers favorable ionic conductivity, low viscosity, and separator wettability, it exhibits poor high-voltage stability (~3.4 V *vs.* Na^+/Na).[11] Introducing low-concentration NaDFOB slightly reduced conductivity due to its lower intrinsic conductivity versus $NaPF_6$, hindered ion migration, and increased viscosity (Fig. 1a and Supplementary Figs. 1−2). Importantly, at this concentration (0.2M), NaDFOB addition fails to satisfactorily enhance the electrolyte's anodic stability limit, primarily because it cannot sufficiently control the structure within the bulk electrolyte and at the cathode interface (Supplementary note 1). Higher NaDFOB concentrations modestly recovered conductivity and further increased viscosity, but

beyond 0.6M, electrolyte cloudiness indicated salt precipitation.".

On page 15 of revised manuscript, we have added the Figure R16 into the Figure 1a.

Question 4. In Figure 3a, NaDFOB decomposes at a low voltage of 2.9 V. Since NaDFOB is a component of the DDSLE, it is not appropriate to claim that the decomposition voltage of this electrolyte is 5.1 V.

Answer: We sincerely appreciate the reviewer's careful reading and insightful comments regarding the decomposition behavior observed in Figure 3a. Upon re-examining the LSV data, we acknowledge that characterizing the overall "decomposition voltage" of the DDSLE solely as 5.1 V is indeed inappropriate and potentially misleading. This is because the LSV profile reveals distinct decomposition stages at different voltages:

(a) Initial anion decomposition: a discernible current increase occurs between 2.9 V and 3.4 V, attributed to the premature oxidative decomposition of the $DFOB^-$ anion. This aligns with Raman peaks (469–1240 cm^{-1}) observed at 3.3–3.7 V, indicative of B/P/C−O/F species.

(b) Solvent decomposition onset: a broader current feature emerges between 3.9 V and 5.1 V, corresponding to the dominant oxidative decomposition of solvent components (EC and EMC). Raman data (2780–2960 cm^{-1}) at 4.3–4.5 V further support this, revealing O−H species formation.

(c) Sustained electrolyte breakdown: beyond ~5.1 V, a sharp near-vertical current rise signifies sustained large-scale decomposition, driven by cumulative breakdown of both anions and solvents under high polarization.

Thus, 5.1 V specifically denotes the onset of accelerated, large-scale decomposition, not the electrolyte's initial decomposition point (which begins at ~2.9 V with $DFOB^-$ degradation).

To accurately reflect this staged decomposition behavior and avoid the ambiguity inherent in the term "decomposition voltage," we have replaced it with more precise descriptions of "anodic stability limit" in revised manuscript.

On page 5 of revised manuscript, we have revised the discussion with "The preferential oxidation of $DFOB^-$, indicated by minor current peaks at 3.0–3.4 V, elevates the anodic stability limit of electrolytes from 3.4 V (BE electrolyte) to 5.1 V (DDSLE electrolyte, Fig. 3a). This enhanced oxidative stability is further confirmed through statistical data and tests on additional substrates (Ni and Al foil) in Na||inert metal coin cells (Supplementary Fig. 11)."

On page 9 of revised manuscript, we have revised the Conclusion with "These synergistic effects significantly enhanced electrolyte stability at high voltages, evidenced by an increased anodic stability limit (from 3.4 V to 5.1 V), improved Coulombic efficiency, reduced over-charging and gaseous release (46.6% reduction)."

All changes are marked in yellow in the revised manuscript for reference.